APL Materials

Broadening microwave absorption via a multi-domain structure

Cite as: APL Mater. **5**, 046104 (2017); https://doi.org/10.1063/1.4979975
Submitted: 01 March 2017 . Accepted: 29 March 2017 . Published Online: 20 April 2017

Zhengwang Liu, Renchao Che, Yong Wei, Yupu Liu, Ahmed A. Elzatahry, Daifallah Al. Dahyan, and Dongyuan Zhao

Broadening microwave absorption via a multi-domain structure

Zhengwang Liu,[1] Renchao Che,[1,a] Yong Wei,[1] Yupu Liu,[1]
Ahmed A. Elzatahry,[2] Daifallah Al. Dahyan,[3] and Dongyuan Zhao[1,a]
[1]*Laboratory of Advanced Materials, Department of Chemistry, Department of Materials Science, iChEM (Collaborative Innovation Center of Chemistry for Energy Materials), Fudan University, Shanghai 200433, China*
[2]*Materials Science and Technology Program, College of Arts and Sciences, Qatar University, P.O. Box 2713, Doha, Qatar*
[3]*Department of Chemistry, King Saud University, Riyadh 11451, Saudi Arabia*

(Received 1 March 2017; accepted 29 March 2017; published online 20 April 2017)

Materials with a high saturation magnetization have gained increasing attention in the field of microwave absorption; therefore, the magnetization value depends on the magnetic configuration inside them. However, the broad-band absorption in the range of microwave frequency (2-18 GHz) is a great challenge. Herein, the three-dimensional (3D) Fe/C hollow microspheres are constructed by iron nanocrystals permeating inside carbon matrix with a saturation magnetization of 340 emu/g, which is 1.55 times as that of bulk Fe, unexpectedly. Electron tomography, electron holography, and Lorentz transmission electron microscopy imaging provide the powerful testimony about Fe/C interpenetration and multi-domain state constructed by vortex and stripe domains. Benefiting from the unique chemical and magnetic microstructures, the microwave minimum absorption is as strong as −55 dB and the bandwidth (<−10 dB) spans 12.5 GHz ranging from 5.5 to 18 GHz. Morphology and distribution of magnetic nano-domains can be facilely regulated by a controllable reduction sintering under H_2/Ar gas and an optimized temperature over 450–850 °C. The findings might shed new light on the synthesis strategies of the materials with the broad-band frequency and understanding the association between multi-domain coupling and microwave absorption performance. [http://dx.doi.org/10.1063/1.4979975]

Magnetic materials have been attracting great attention in the fields of absorption and separation,[1–3] drug delivery,[4,5] microwave absorption,[6] optical isolator,[7] and so on, owing to the fast response to the external static and alternating field, which are endowed by the high saturation magnetization. When the sizes are down to nanoscale, the materials exhibit low remnant magnetization and unique electric properties, facilitating multi-band microwave absorption;[8–10] however, their saturation magnetizations substantially decrease suffering from the magnetic disorder on the surface and chemical corrosion during the usage, limiting widening and enhancement of microwave absorption. In this context, many efforts have been made towards the synthesis of unique nanomaterials with strong and broad-band microwave absorption. For example, the protective-shell strategies, i.e., coating with organic species or inorganic layers, have been developed to chemically stabilize the naked nanomaterials against the degradation of properties.[11–16] In addition, owing to the fact that the size and shape-dependent anisotropy energy dominates the magnetic properties, many attempts have been oriented towards the hierarchical-structure design of materials.[17–24] Briefly, although the properties of nanomaterials can be retained or enhanced by the above-mentioned strategies, it is still difficult to widen the microwave absorption band.

[a]Electronic addresses: rcche@fudan.edu.cn and dyzhao@fudan.edu.cn. URL: http://www.mesogroup.fudan.edu.cn.

As we know, it is the magnetic configurations that govern the properties, such as saturation magnetization. In general, they consist of a single-domain state, vortex and multi-domain state, resulting from the minimization of total energy, including magneto-crystalline anisotropy, exchange energy, and size and shape-dependent anisotropy.[25] The different states are endowed with unique applications. For example, the single domain state is often suitable for the devices requiring high coercivity, such as hard disk drives[26] and permanent magnets;[27] the vortex state is useful for biomedicines, such as hyperthermia[28] and drug delivery,[29] owing to the minimization of stray field and the inhibition of aggregation between materials; the multi-domain state can be applied to the data storage,[30] profiting from the domain wall motion. At present, the natural resonance of the states has already been recognized as a key microwave absorption mechanism. Moreover, their resonance frequency depends on the size, shape, and coupling of the states, therefore, the multi-domain state, which is endowed with the versatile size, shape, and coupling, can help to widen the microwave absorption band. However, the states can but be formed under a low temperature and extra field,[30,31] except for ultrathin nanoscaled Pt/Co/MgO heterostructures.[32] Hence, it is a great challenge to form the state under room temperature and zero-magnetic field, which is a key to improve the microwave absorption performance.

Herein, we report unique Fe/C hollow microspheres (Fe/C HMs) with 3D Fe/C interpenetrating networks and multi-domain state inside the wall by a simple H_2/Ar gas reduction, evidenced by electron tomography, electron holography, and Lorentz TEM imaging. The saturation magnetization of the Fe/C HMs was measured to be 340 emu/g, much larger than that of bulk metal Fe, unexpectedly. The bandwidth (≤ -10.0 dB) at 2.5 mm in thickness is as wide as 12.5 GHz ranging from 5.5 to 18 GHz. The multi-domain state could effectively broaden the absorbable frequency band by natural and exchange resonance effects, paving a way to the materials with the excellent microwave absorption and high density storage.

Fe-containing organometallic precursors with uniform microspheres were prepared by using a solvothermal method;[33] the detailed preparation procedures were listed in the Experimental Section (see the supplementary material) and the illustration of reaction equipment was presented (Scheme 1(a)). The SEM images (Figs. 1(a) and 1(b)) show that the organometallic precursors have hollow microspherical structures with the diameter of ~7 μm, which are self-assembled by the nanosheets (Fig. S1). After a calcination ranging from 450 to 850 °C under a H_2/Ar gas flow (the detailed calcination parameters were listed in the Experimental Section (see the supplementary material)) and the illustration of reaction unit was presented (Scheme 1(b)), the hollow spherical structure is basically retained (Figs. 1(d)–1(i)). However, with increasing calcination temperature from 450 to 850 °C, the nano-sheets located outside the hollow microspheres gradually disappear and the diameter decreases from 4.5 to 3.0 μm (Figs. 1(d)–1(l), Fig. S2). The hollow structural feature is further confirmed by the broken microspheres (Figs. 1(e), 1(h), and 1(k)), which is similar with the metallic Pt open-mouthed microcapsule.[34] Thereinafter, we focus on the three samples obtained under the reduction temperature (450, 650, and 850 °C), denoted as Fe/C HM-450, Fe/C HM-650, and Fe/C HM-850, respectively. The XRD patterns of the samples obtained under the reduction temperature (Fig. S3) show the three diffraction peaks at 44.7°, 65.0°, and 82.3°, which can be indexed to the (110), (200), and (211) planes of α-Fe (JCPDS card no. 65-4899) and the other two peaks at 14.8°

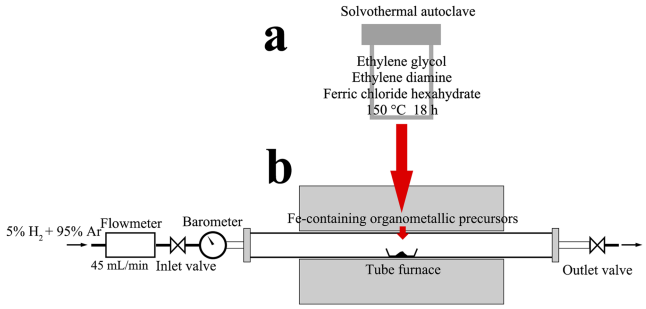

SCHEME 1. The illustration for the preparation process of the Fe/C hollow microspheres.

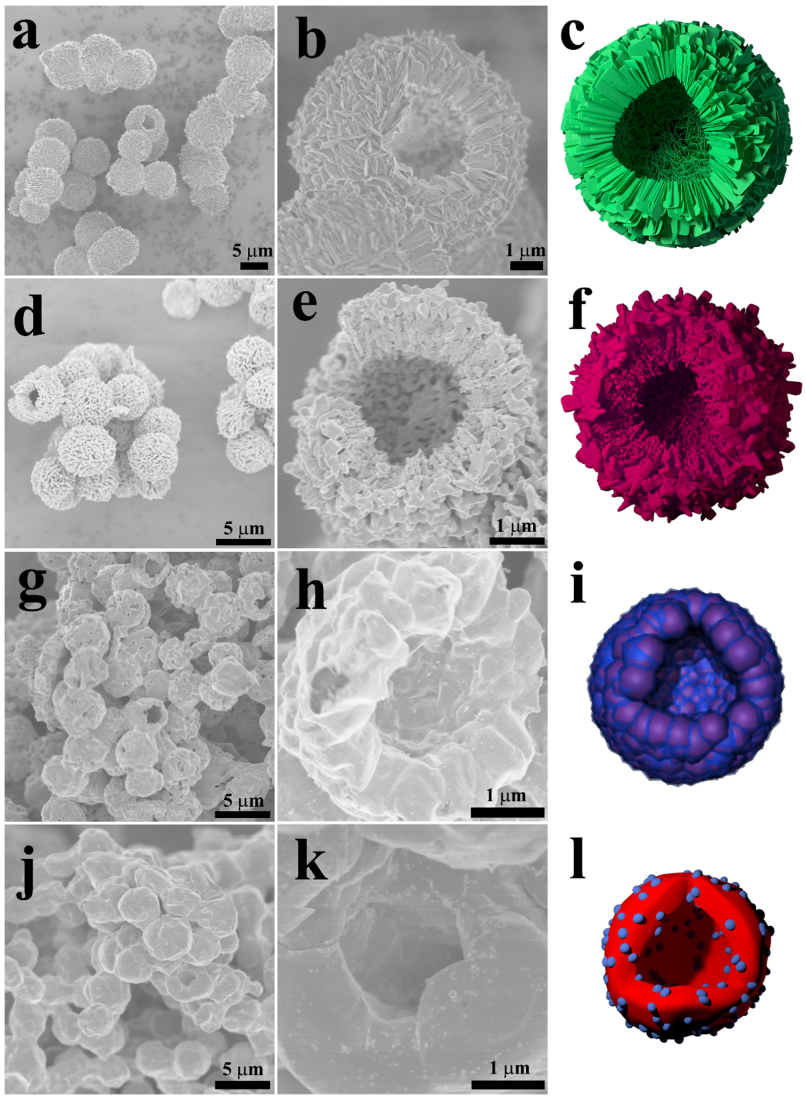

FIG. 1. The SEM images of the Fe-containing organometallic microspheres ((a) and (b)) and Fe/C hollow microspheres prepared at different reduction temperatures: 450 °C ((d) and (e)), 650 °C ((g) and (h)), and 850 °C ((j) and (k)); the models of the Fe-containing organometallic microsphere (c), showing a hollow sphere with the randomly assembled nano-sheets on the wall; and Fe/C hollow microspheres prepared at different reduction temperatures: 450 °C (f), showing a hollow sphere with the shrunken and cross-linking nano-sheets on the wall; 650 °C (i), showing a hollow sphere with the 3D compact Fe/C distribution on the wall; and 850 °C (l), showing a hollow sphere with the discrete Fe/C distribution on the wall.

and 29.9° are from the (001) and (002) planes of the graphite carbon (JCPDS card no. 89-8490). It is revealed by TEM images that the annealing temperatures can influence the microstructure of the spherical walls. At low (450 °C) and middle (650 °C) reduction temperatures, the TEM images (Figs. 2(a) and 2(b) (Multimedia view)) of the walls from the Fe/C hollow microspheres show that the iron nanoparticles are coated by the graphitic carbon layers. Moreover, the 3D element distribution analysis over a part of the Fe/C hollow microsphere suggests that the iron nanoparticles (the inside core with red color in Fig. 2(d) (Multimedia view)) are dominantly mixed or wrapped by randomly distributed carbon (the outside core with blue color in Fig. 2(d) (Multimedia view)), the 3D element distribution electron tomography is given as a Multimedia view in Fig. 2. Thus, a 3D inter-penetrating Fe/C hollow microsphere is confirmed to be successfully formed by the annealing under H_2/Ar gas atmosphere. However, at a high temperature (850 °C), the SEM image (Fig. S4) of the Fe/C hollow microspheres shows some nanoparticles located on the surface of the walls. The TEM image (Fig. 2(c) (Multimedia view)) reveals that the nanoparticles are situated outside the

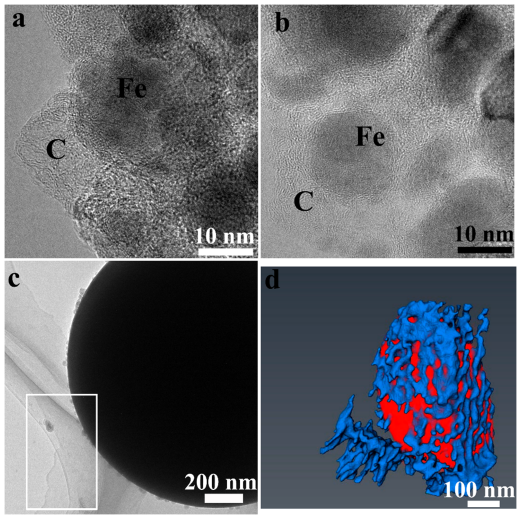

FIG. 2. The TEM images of the Fe/C hollow microspheres prepared at different reduction temperatures: 450 °C (a), 650 °C (b), and 850 °C (c) and the 3D EDS from the wall of the Fe/C hollow microspheres prepared at 650 °C (d), which were obtained by the electron tomography with 3D EDS detector; the outside shell with blue color denotes carbon element and the inside core with red color denotes iron element. (Multimedia view) [URL: http://dx.doi.org/10.1063/1.4979975.1]

surface. The EDS (Energy-Dispersive X-ray Spectroscopy) mapping (Fig. S5) in the white rectangle of Fig. 2(c) (Multimedia view) simultaneously proves that the chemical composition of the nanoparticles is only carbon element, suggesting that the massive carbon inside the Fe/C hollow microspheres is "squeezed" out from the walls. Raman spectrum (Fig. S7) of the Fe/C HM-650 shows two bands at 1335 and 1558 cm^{-1}, which could be ascribed to D and G bands of graphitic carbon, respectively. D band is indicative of the graphitic carbon with the structural defect,[35] leading to a dielectric loss to the microwave propagation.

Saturation magnetization (Ms) of the Fe/C hollow microspheres prepared at 450 and 850 °C was measured to be 167 and 197 emu/g, respectively (hysteresis loops in Fig. 3(a)), both values are smaller than that of the bulk metal Fe (220 emu/g).[36] Surprisingly, Ms of the Fe/C hollow microspheres prepared at 650 °C can reach as high as 340 emu/g, which is 1.55 times as that of the bulk Fe, meanwhile, both the coercivity and remnant magnetization are the lowest value among these samples (Table I). As we know, in the process of technical magnetization, the rotation and wall displacement of the domain contribute to the enhancement of the saturation magnetizations,[37] in which, the displacement is more beneficial to the increase of Ms and the decrease of coercivity and remnant magnetization. Therefore, the sample Fe/C HM-650 should contain the sufficient domain wall compared to that of the other two samples.

The magnetic microstructure of the samples was clarified by Lorentz TEM, and its contrast was induced by the Lorentz force ($F = q \cdot (v \times B)$, where q and v are electron charge and velocity, respectively, and B is the magnetic flux density). The electron beam through the intrinsic magnetic field of the specimen could deflect away from its original path, thus increasing or decreasing the beam irradiation intensity at the inter-domain. Briefly, the magnetic microstructure contrast depends sensitively on the interaction between TEM electron beam and the intrinsic magnetization field from the sample. Lorentz TEM images of the thin lamellar toroid samples (Figs. S8-S10 of the supplementary material) show the inverse of white/black line, resulting from the fact that magnetic domains deflect the electron beam by Lorentz force. The magnetization vector maps (Figs. 3(c)–3(e)) can be directly obtained from three Lorentz TEM images (under-focus, in-focus, and over-focus) with the aid of transport of intensity equation (TIE)[38] using QPt plugin in the Gatan DM software; obviously, the inner state of the sample Fe/C HM-650 is the multi-domain with average size of about 250 nm (Fig. 3(c)), moreover, areas I, II, and III in Fig. 3(c) contain cross-tie wall (Fig. 3(c–I)), Neel wall (Fig. 3(c–II)), and Bloch wall (Fig. 3(c–III)), respectively. It is evident that magnetization vectors of cross-tie wall rotate 90° within the plane (Fig. 3(c–I)), forming a vortex domain; magnetization vectors of Neel wall rotate in the plane (Fig. 3(c–II)); magnetization vectors of Bloch wall give

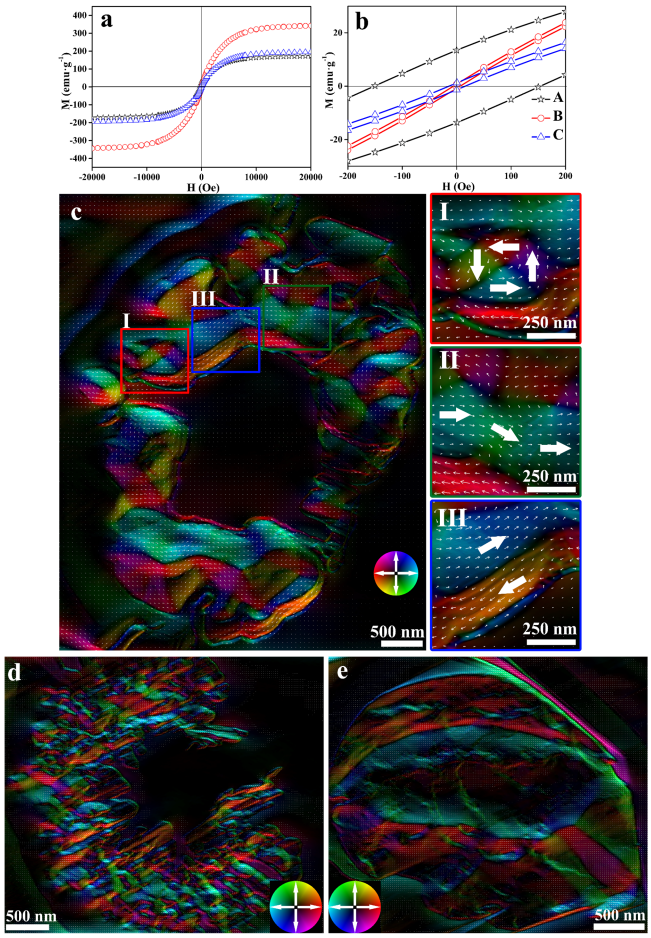

FIG. 3. The hysteresis loops ((a) and (b)) of the Fe/C hollow microspheres prepared at different reduction temperatures: 450 °C (A), 650 °C (B), and 850 °C (C); the magnetization vector maps of the Fe/C hollow microspheres prepared at different reduction temperature: 450 °C (d), 650 °C (c), and 850 °C (e); I, II and III were the magnified picture of area I, II and III in Fig. 3(b), the color wheels (bottom corner in Figs. 3(c)–3(e)) indicated the direction (from the center to a point) and intensity (the deeper the color is, the stronger the intensity is) of in-plane magnetization at each point, and the white arrows (Figs. 3(c–I)) represented the magnetization direction at their location.

rise to an out-plane rotation (Fig. 3(c–III)). All the three types of domains coexist and couple with each other, contributing to a high *Ms* (340.0 emu/g), low coercivity, and remnant magnetization.[39] Comparatively, the state of the sample Fe/C HM-450 is seemingly stripe multi-domain with ~200 nm in size, which is equal to the thickness of the discrete Fe/C sheets (Fig. S9(b)); however, excluding the influence of free space between the separated C/Fe sheets (the red frame in Fig. S9(b)), the domains should be the single stripe structure on the magnetization vector maps (Fig. 3(d)). Obviously, the structures of the sample C/Fe HM-850 (Fig. 3(e)) are basically stripe multi-domain with 500 nm in size. It is well known that when a magnetic domain is formed, positive and negative magnetic-charge can be localized at the two ends, giving rise to stray field. The electron holography image (Fig. S12)

TABLE I. The static magnetic properties of Fe/C hollow microspheres.

	Saturation magnetization (*Ms*) emu/g	Coercivity (Hc) Oe	Remanent magnetization (*Br*) emu/g
Fe/C HM-450	167.0	152.0	14.0
Fe/C HM-650	340.0	6.0	0.8
Fe/C HM-850	194.0	15.0	1.1

of the sample Fe/C HM-650 unveils that the hollow structure can generate a high density of stray magnetic flux closure lines from the multi-domain, furthermore, the density of intra-cavity is higher than that of extra-cavity.

The color bar on the right side of the 3D RL (reflection loss) plots of Fe/C hollow microspheres prepared at different reduction temperatures, 450, 650, and 850 °C (Fig. 4), represents the RL intensity: the yellow and blue areas represent that the RL is less than −10.0 dB. When the thickness is between 2.0 and 5.0 mm, the yellow and blue areas of the sample Fe/C HM-450 (Fig. 4(a)) exhibit the dual-band absorption under the fixed thickness. With increasing thickness, the dual-band absorption moves to low frequency. Within the range of 2.0–5.0 mm in thickness, the dual-band absorption (≤−10.0 dB) of the sample Fe/C HM-650 (the yellow and blue areas in Fig. 4(b)) becomes strong, moreover, its bandwidth is wider than that of Fe/C HM-450; therefore, within the range of 2.0–3.0 mm in thickness, the dual-band overlaps with each other. Compared with the microwave absorption of the samples Fe/C HM-450 and Fe/C HM-650, the absorption bandwidth (≤−10.0 dB) of Fe/C HM-850 (Fig. 4(b)) is obviously narrower. In order to directly compare RL of the three Fe/C HMs under the same 2.5 mm in thickness, the minimum RL values (Fig. 4(d)) of Fe/C HM-450, Fe/C HM-650, and Fe/C HM-850 are −34.0 dB at 8.0 GHz, −27.0 dB at 7.0 GHz, and −15 dB at 13.0 GHz, respectively. The absorption bandwidth (≤−10.0 dB) of Fe/C HM-650 (Fig. 4(d)) is 12.5 GHz ranging from 5.5 to 18 GHz at 2.5 mm in thickness, wider than that of the other two samples.

Based on the above results, the high saturation magnetization, low coercivity, and remnant magnetization of the Fe/C hollow microspheres benefit from the synergistic effects between the compact 3D Fe/C interpenetrating networks and hollow structure, rather than the loosened 3D Fe/C interpenetrating networks or the discrete Fe/C distribution. Just with the assistance of these features, the multi-domain state and disperse stray field are successfully formed. As we know,[40–42]

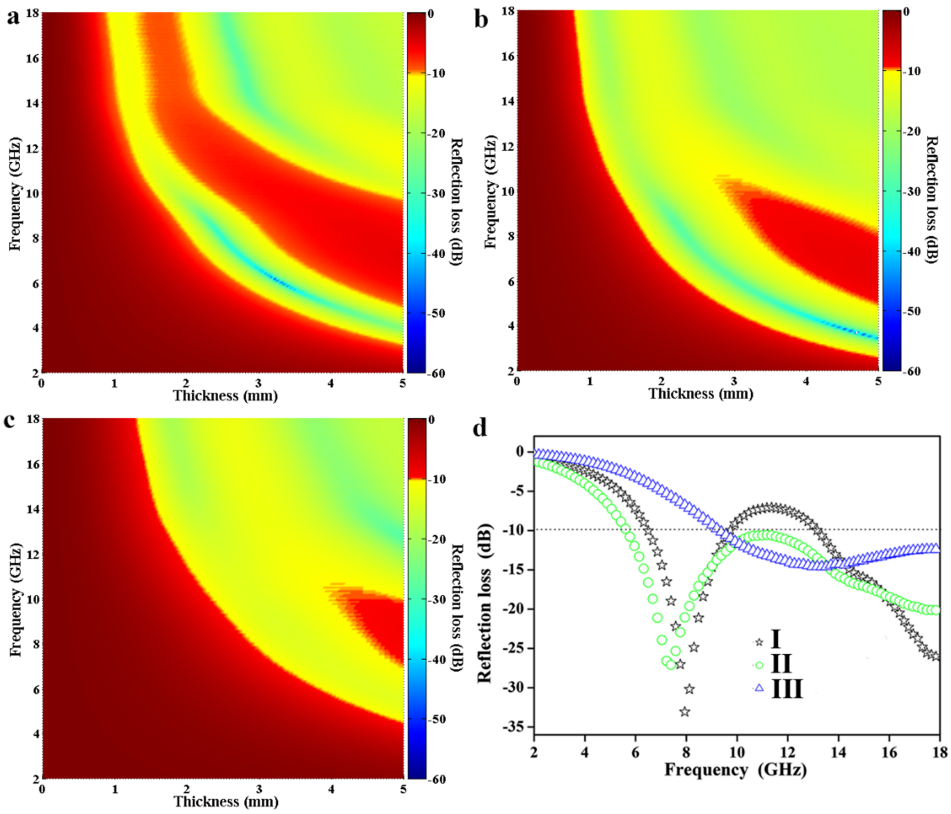

FIG. 4. The 3D RL plots of the Fe/C hollow microspheres prepared at different reduction temperatures: at 450 °C (a), 650 °C (b), and 850 °C (c), frequency (2-18 GHz) versus thickness (0.1-5 mm); the RL curves (d) versus frequency (2-18 GHz) of Fe/C hollow microspheres at different reduction temperatures: 450 °C (I), 650 °C (II), and 850 °C (III), in which the thickness of all three samples were 2.5 mm.

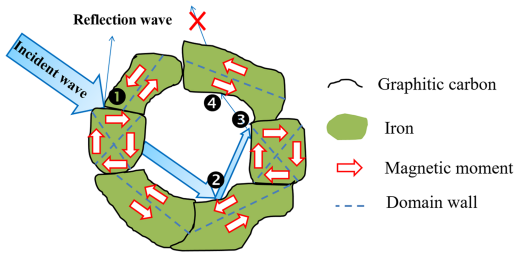

SCHEME 2. The microwave absorption mechanism of the Fe/C hollow microspheres.

the effective field of a domain depends on the shape, size, and surrounding. Therefore, the Fe/C hollow microspheres with the unique structure can possess the broad effective fields and natural and exchange resonance frequency, furthering the ultra-band microwave absorption. Meanwhile, the 3D interpenetrating Fe/C networks can not only contribute the abundant Fe/C interfaces, thus providing interfacial polarization relaxation, but also stabilize the multi-domain state. Therefore, the microwave absorption mechanism (Scheme 2) is proposed that on the ❶ surface of Fe/C hollow microspheres, an incident microwave interacts with the Fe/C interfaces, generating the microwave attenuation due to interface and defect dipole polarization and electron hopping conductivity; then, the microwave excites the natural and exchange resonance of magnetic moments in the domains of the Fe/C hollow microsphere, along with the microwave dissipation from the damping factors of the 3D Fe/C networks with defects; subsequently, due to multiple reflections by the hollow cavity, the above process on the ❶ surface similarly takes place on the other ❷ ❸ ❹ surfaces (Scheme 2); finally, the microwave with broad-band frequency could be effectively absorbed.

According to alternating current (AC) impedance spectroscopy,[43] if a semicircle appears in the Nyquist plot, the resistor and capacitor (positive value Zin'') or resistor and inductor (minus value Zin'') are connected in a parallel way. The Nyquist plot (Zin'' versus Zin') of Fe/C HM-650 (Fig. S11 of the supplementary material) shows three semicircles with positive and minus value Zin'', demonstrating that in the equivalent circuit of microwave absorption (inset of Fig. S11), the resistors (intrinsic resistance of carbon and iron), capacitors (interfaces from inter-grain of carbon and iron), and inductors (magnetic multi-domain) are connected in parallel. First, the intrinsic resistance of carbon and iron provides resistance loss. Second, the Fe/C interfaces contribute interfacial relaxation polarization and loss. Third, the multi-domain generates natural resonance. Moreover, the three circuit components can possess different values at each micro-area, thus broadening natural resonance frequency and absorption band. In addition, the parallel connections among the three circuit components could induce micro-circuit resonance, further widening natural resonance frequency and the absorption band.

3D Fe/C hollow microspheres with the multi-domain state were fabricated by the high temperature reduction of Fe-containing organometallic precursor hollow microspheres with 5% H_2/Ar gas. At 650 °C, the multi-domain state in the wall of Fe/C hollow microspheres is formed and stabilized by 3D Fe/C interfaces. Owing to the state, the Fe/C hollow microspheres are endowed with high Ms and low coercivity and remnant magnetization, thus exhibiting strong microwave absorption property with a bandwidth as wide as 12.5 GHz (RL < −10 dB). The dynamic magnetization of the multi-domain was confirmed to be the key microwave absorption mechanism of the ultra-broad band by electron tomography, electron holography, and Lorentz TEM. This work might pave a way for ultra-broad absorption band and high density storage.

See supplementary material for the experimental methods, the microstructural characterization and electromagnetic parameters of the Fe/C hollow microspheres.

This work was supported by the Ministry of Science and Technology of China (973 Project Nos. 2013CB932901 and 2016YFE0105700) and the National Natural Science Foundation of China (Nos. 51672050 and 51172047) and NSAF-U1330118. The authors extend their appreciation to the International Scientific Partnership Program ISPP at King Saud University for funding this research work through ISPP# 0018.

[1] J. Guo, W. L. Yang, and C. C. Wang, Adv. Mater. **25**, 5196 (2013).
[2] J. Liu, S. Z. Qiao, Q. H. Hu, and G. Q. Lu, Small **7**, 425 (2011).
[3] D. H. K. Reddy and Y. S. Yun, Coord. Chem. Rev. **315**, 90 (2016).
[4] B. Luo, S. A. Xu, A. Luo, W. R. Wang, S. L. Wang, J. Guo, Y. Lin, D. Y. Zhao, and C. C. Wang, ACS Nano **5**, 1428 (2011).
[5] K. Ulbrich, K. Holá, V. Šubr, A. Bakandritsos, J. Tuček, and R. Zbořil, Chem. Rev. **116**, 5338 (2016).
[6] Q. H. Liu, Q. Cao, H. Bi, C. Y. Liang, K. P. Yuan, W. She, Y. J. Yang, and R. C. Che, Adv. Mater. **28**, 486 (2015).
[7] A. Kawashima, T. Nakanishi, Y. Kitagawa, K. Fujita, K. Tanaka, K. Fushimi, M. A. Malik, P. O'Brien, and Y. Hasegawa, Bull. Chem. Soc. Jpn. **88**, 1453 (2015).
[8] X. Gu, W. M. Zhu, C. J. Jia, R. Zhao, W. Schmidt, and Y. Q. Wang, Chem. Commun. **47**, 5337 (2011).
[9] Y. H. Chen, Z. H. Huang, M. M. Lu, W. Q. Cao, J. Yuan, D. Q. Zhang, and M. S. Cao, J. Mater. Chem. A **3**, 12621 (2015).
[10] W. M. Zhu, L. Wang, R. Zhao, J. W. Ren, G. Z. Lu, and Y. Q. Wang, Nanoscale **3**, 2862 (2011).
[11] W. Li, Y. H. Deng, Z. X. Wu, X. F. Qian, J. P. Yang, Y. Wang, D. Gu, F. Zhang, B. Tu, and D. Y. Zhao, J. Am. Chem. Soc. **133**, 15830 (2011).
[12] W. Li, J. P. Yang, Z. X. Wu, J. X. Wang, B. Li, S. S. Feng, Y. H. Deng, F. Zhang, and D. Y. Zhao, J. Am. Chem. Soc. **134**, 11864 (2012).
[13] L. S. Lin, Z. X. Cong, J. B. Cao, K. M. Ke, Q. L. Peng, J. H. Gao, H. H. Yang, G. Liu, and X. Y. Chen, ACS Nano **8**, 3876 (2014).
[14] J. W. Liu, J. J. Xu, R. C. Che, H. J. Chen, M. M. Liu, and Z. W. Liu, Chem. Eur. J. **19**, 6746 (2013).
[15] J. W. Liu, R. C. Che, H. J. Chen, F. Zhang, F. Xia, Q. S. Wu, and M. Wang, Small **8**, 1214 (2012).
[16] W. C. Zhou, X. J. Hu, X. X. Bai, S. Y. Zhou, C. H. Sun, J. Yan, and P. Chen, ACS Appl. Mater. Interfaces **3**, 3839 (2011).
[17] Q. H. Liu, Q. Cao, X. B. Zhao, H. Bi, C. Wang, D. S. Wu, and R. C. Che, ACS Appl. Mater. Interfaces **7**, 4233 (2015).
[18] G. B. Sun, B. X. Dong, M. H. Cao, B. Q. Wei, and C. W. Hu, Chem. Mater. **23**, 1587 (2011).
[19] J. Liu, Z. K. Sun, Y. H. Deng, Y. Zou, C. Y. Li, X. H. Guo, L. Q. Xiong, Y. Gao, F. Y. Li, and D. Y. Zhao, Angew. Chem., Int. Ed. **48**, 5875 (2009).
[20] X. L. Cheng, J. S. Jiang, D. M. Jiang, and Z. J. Zhao, J. Phys. Chem. C **118**, 12588 (2014).
[21] C. J. Jia, L. D. Sun, F. Luo, X. D. Han, L. J. Heyderman, Z. Yan, C. H. Yan, K. Zheng, Z. Zhang, M. Takano, N. Hayashi, M. Eltschka, M. Kläui, U. Rüdiger, T. Kasama, L. Cervera Gontard, R. E. Dunin Borkowski, G. Tzvetkov, and J. Raabe, J. Am. Chem. Soc. **130**, 16968 (2008).
[22] T. Wang, H. Wang, X. Chi, R. Li, and J. Wang, Carbon **74**, 312 (2014).
[23] R. Qiang, Y. C. Du, H. T. Zhao, Y. Wang, C. H. Tian, Z. G. Li, X. J. Han, and P. Xu, J. Mater. Chem. A **3**, 13426 (2015).
[24] S. L. Zhang, Q. Z. Jiao, Y. Zhao, H. S. Li, and Q. Wu, J. Mater. Chem. A **2**, 18033 (2014).
[25] C. Gatel, F. J. Bonilla, A. Meffre, E. Snoeck, B. Warot-Fonrose, B. Chaudret, L. M. Lacroix, and T. Blon, Nano Lett. **15**, 6952 (2015).
[26] N. Liakakos, T. Blon, C. Achkar, V. Vilar, B. Cormary, R. P. Tan, O. Benamara, G. Chaboussant, F. Ott, B. Warot Fonrose, E. Snoeck, B. Chaudret, K. Soulantica, and M. Respaud, Nano Lett. **14**, 3481 (2014).
[27] K. Gandha, K. Elkins, N. Poudyal, X. B. Liu, and J. P. Liu, Sci. Rep. **4**, 5345 (2014).
[28] X. L. Liu, Y. Yang, C. T. Ng, L. Y. Zhao, Y. Zhang, B. H. Bay, H. M. Fan, and J. Ding, Adv. Mater. **27**, 1939 (2015).
[29] D. Ho, X. L. Sun, and S. H. Sun, Acc. Chem. Res. **44**, 875 (2011).
[30] N. Biziere, C. Gatel, R. Lassalle Balier, M. C. Clochard, J. E. Wegrowe, and E. Snoeck, Nano Lett. **13**, 2053 (2013).
[31] X. Z. Yu, Y. Onose, N. Kanazawa, J. H. Park, J. H. Han, Y. Matsui, N. Nagaosa, and Y. Tokura, Nature **465**, 901 (2010).
[32] O. Boulle, J. Vogel, H. Yang, S. Pizzini, D. de Souza Chaves, A. Locatelli, T. O. Menteş, A. Sala, L. D. Buda-Prejbeanu, O. Klein, M. Belmeguenai, Y. Roussigné, A. Stashkevich, S. M. Chérif, L. Aballe, M. Foerster, M. Chshiev, S. Auffret, I. M. Miron, and G. Gaudin, Nat. Nanotechnol. **11**, 449 (2016).
[33] B. Wang, H. B. Wu, L. Zhang, and X. W. Lou, Angew. Chem., Int. Ed. **52**, 4165 (2013).
[34] S. Mandal, M. Sathish, G. Saravanan, K. K. R. Datta, Q. Ji, J. P. Hill, H. Abe, I. Honma, and K. Ariga, J. Am. Chem. Soc. **132**, 14415 (2010).
[35] X. F. Zhang, P. F. Guan, and X. L. Dong, Appl. Phys. Lett. **96**, 223111 (2010).
[36] H. L. Lv, X. H. Liang, Y. Cheng, G. B. Ji, D. M. Tang, B. S. Zhang, H. Q. Zhang, and Y. W. Du, RSC Adv. **5**, 25936 (2015).
[37] R. C. O'Handley, *Modern Magnetic Materials: Principles and Applications* (Wiley, New York, USA, 1999).
[38] M. Reed Teague, J. Opt. Soc. Am. **73**, 1434 (1983).
[39] Q. H. Liu, X. H. Xu, W. X. Xia, R. C. Che, C. Chen, Q. Cao, and J. G. He, Nanoscale **7**, 1736 (2015).
[40] G. Viau, F. Fiévet Vincent, F. Fiévet, P. Toneguzzo, F. Ravel, and O. Acher, J. Appl. Phys. **81**, 2749 (1997).
[41] B. D. Cullity and C. D. Graham, *Introduction to Magnetic Materials* (Wiley, Hoboken, New Jersey, USA, 2009).
[42] S. T. Jiang and W. Li, *Condensed Matter Physics Magnetism* (Science Press, Beijing, China, 2006).
[43] J. R. M. Evgenij Barsoukov, *Impedance Spectroscopy: Theory, Experiment, and Applications* (Wiley, Hoboken, New Jersey, USA, 2005).